APO Imager Preliminary Design Review Technical Document

J. Huehnerhoff
October 15, 2013

1. Introduction

This document is a technical overview of the items that will be presented during the Preliminary Design Review for the new APOImager. Purpose for building this imager, Science Goals, Schedule, and Cost will be discussed in other documents.

2. Optics

To set a metric for the optical design it is first necessary to know the performance that must be reached. This can be accomplished by looking at the expected focal ratio and best seeing conditions. The optical design was able to accomplish a focal reduction from f/10.3 to f/8.0 with reasonable lens constraints and performance. Resulting in a plate scale of 0.007367 "/μm, using equation 1. The ideal pixel size (or minimum spot diameter) can be found by knowing that each image should be Nyquist sampled at the best possible seeing, 0.6". Equation 2 yields an ideal pixel as 40.7μm. Since we are stuck with a pixel size of 15μm this means the optics will be the limiting factor in performance. Even though the ideal pixel size will dictate the optical performance it is necessary to state that the plate scale for this CCD will be 0.111"/pixel. The field of view will be 7.4 arc minutes across the CCD and 10.46 arc minutes across the diagonals. Figure 1a shows the maximum spot radius, while being Nyquist sampled, for a given FWHM of a point source gaussian. This will be useful when measuring the performance of the optics compared to real world observing conditions.

$$plate\ scale = \frac{206265}{aperture(mm) * f/\# * 1000} \frac{arcsecond}{\mu m} \tag{1}$$

$$ideal\ pixel = \frac{1000 * f/\# * aperture(mm) * 0.3}{206265} \frac{\mu m}{pixel} \tag{2}$$

The designed focal reducer consists of three elements closely spaced together, figure 2. The labeling for these elements will increment from right (closest to telescope) to left (closest to CCD) being named: L1, L2, and L3.

Fig. 1.—

(a) Seeing Basis

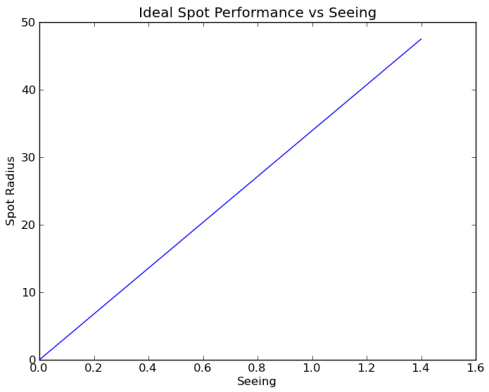

(b) Spot Size Definition

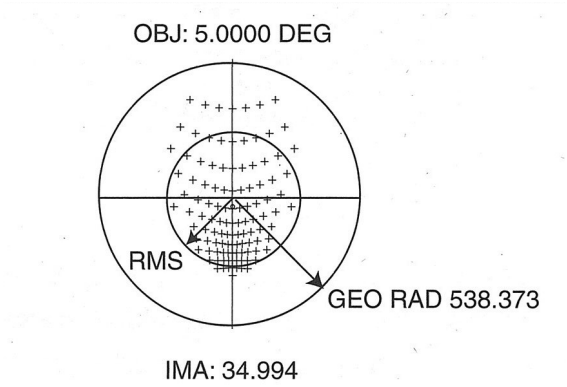

Fig. 2.—: Focal Reducer Layout

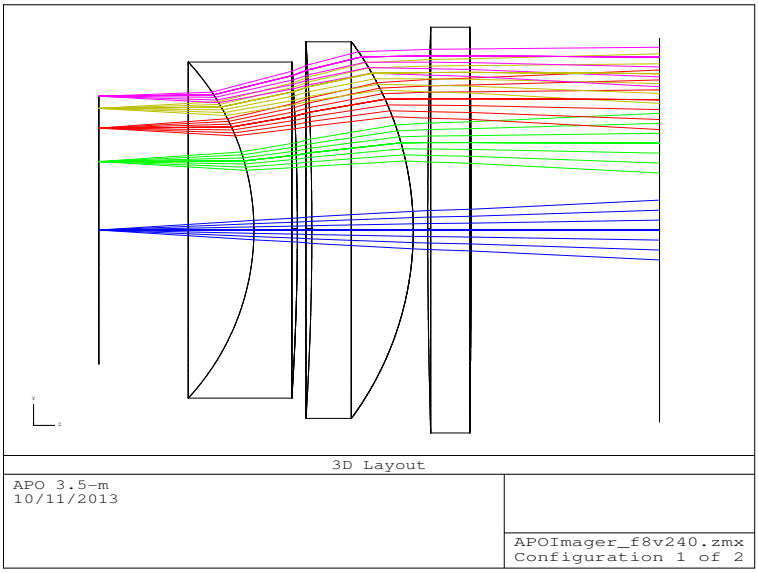

The spot diagram, figure 3, is the expected plot of optical performance. Fields 1, 2, and 3 are points inside a circle enclosed within the CCD, while fields 4 and 5 are points within a circle enclosing the CCD. This spot diagram is in reference to the chief ray in the optical system. Using a centroid based spot radius shows improved results (this would be what the CCD would detect) but the chief ray reference is a good indicator for science programs requiring high astrometric accuracy. The spot radius can be compared to figure 1a. The minimum spot radius, to properly sample the f/8.0 beam, is 20.35μm. It is seen that the RMS radius, across the entire field, is very close to this ideal number. The geometric radius (see figure 3 for definition) is a little larger but will be minimized when looking through smaller band passes. Only when seeing is very good will the geometric radius be larger than the ideal sampling. With standard seeing at APO around 1.1" the geometric radius will be well sampled. Optical performance starts to degrade towards the diagonal corners of the CCD. This was a considered a compromise to get better performance over the central, more scientifically useful, areas.

Fig. 3.—: Spot Diagram

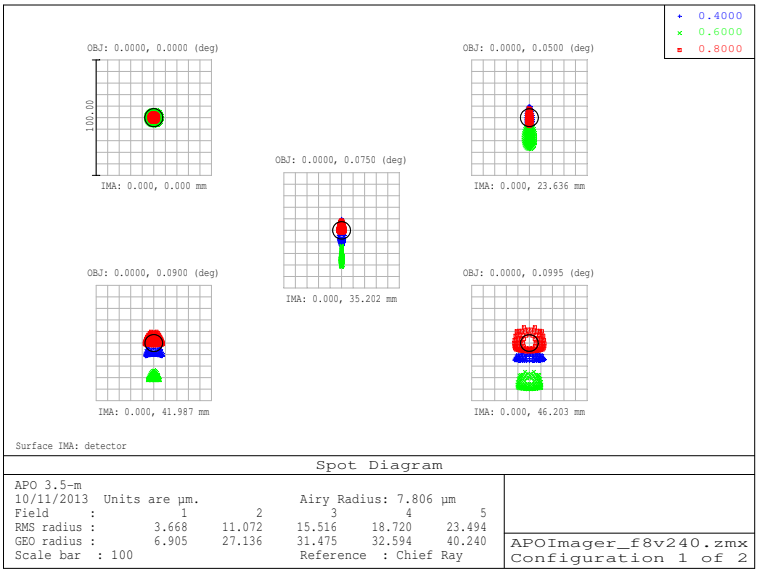

The glass types used on L1, L2, and L3 are SK16, SK14, and F2 (respectively) from Schott. Figure 4 shows the transmittance of these glass types as well as the total expected throughput due to glass. The transmittance numbers have been corrected for glass thickness. Although the combined throughput in the blue is decreased by use of glass, the glass types where chosen due to the higher than average blue throughput.

Figures 5 - 9 show the various individual performance aspects of the optical design. The chromatic focal shift is well controlled across the field. Field curvature is also greatly reduced,

(a) Transmittance 300nm - 1100nm (b) Transmittance 300nm - 400nm

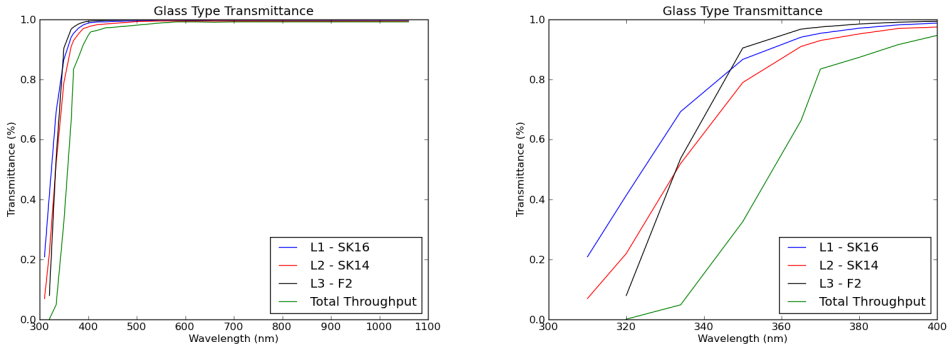

Fig. 4.—: Glass Transmittance Curves

compared to the native telescope 3.5mm. Distortion is significantly worse than the native telescope numbers, but the distortion is a convolved part of the spot diagram. Astigmatism is the worst residual aberration, as can be seen in table 1 and figure 9.

Fig. 5.—: Spot Diagram Through Focus

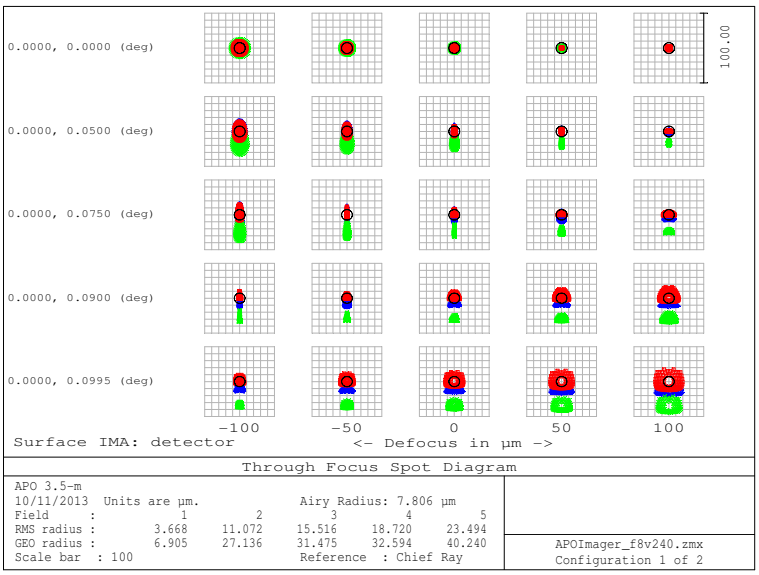

Fig. 6.—: Chromatic Focal Shift

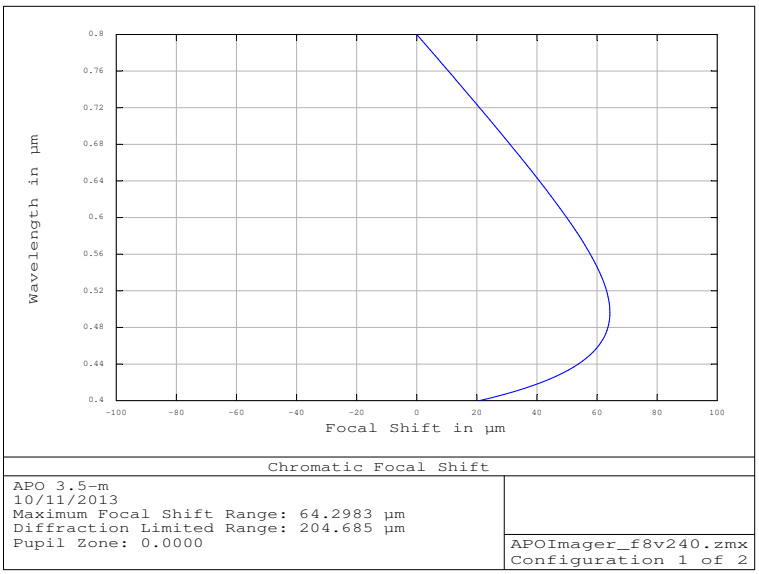

Fig. 7.—: Field Curvature and Distortion

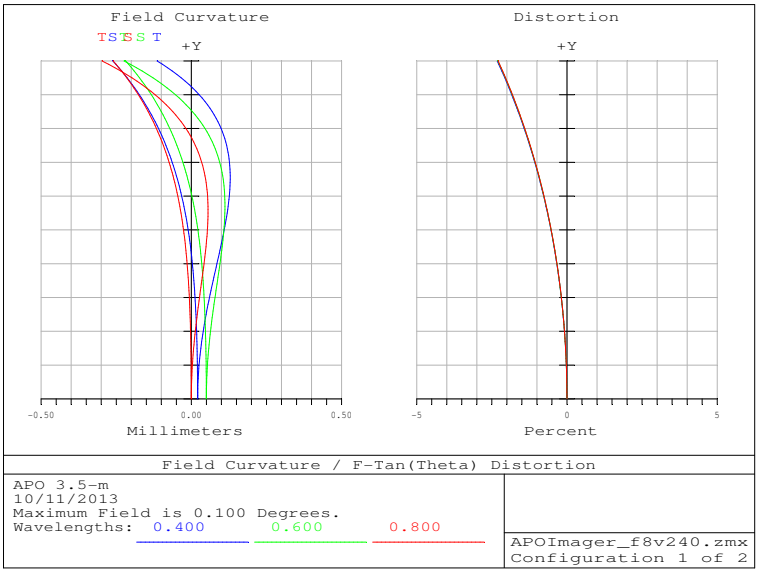

Fig. 8.—: Geometric Encircled Energy

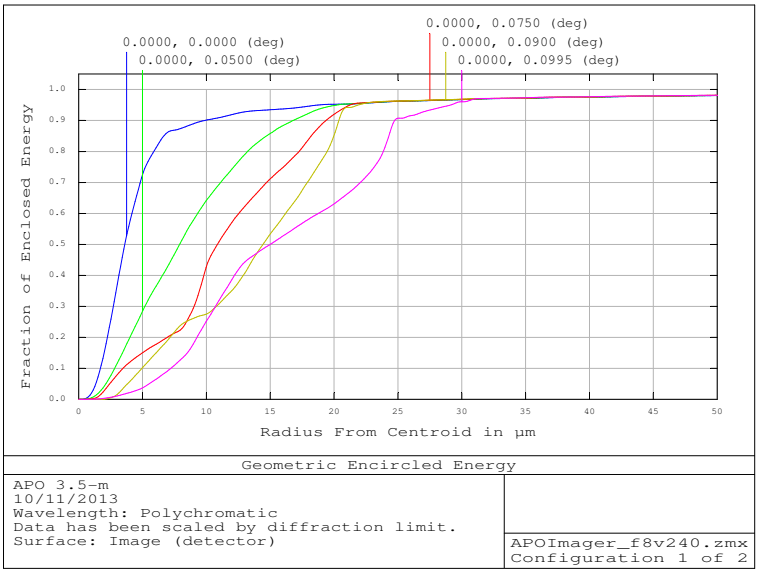

Fig. 9.—: Seidel Diagram

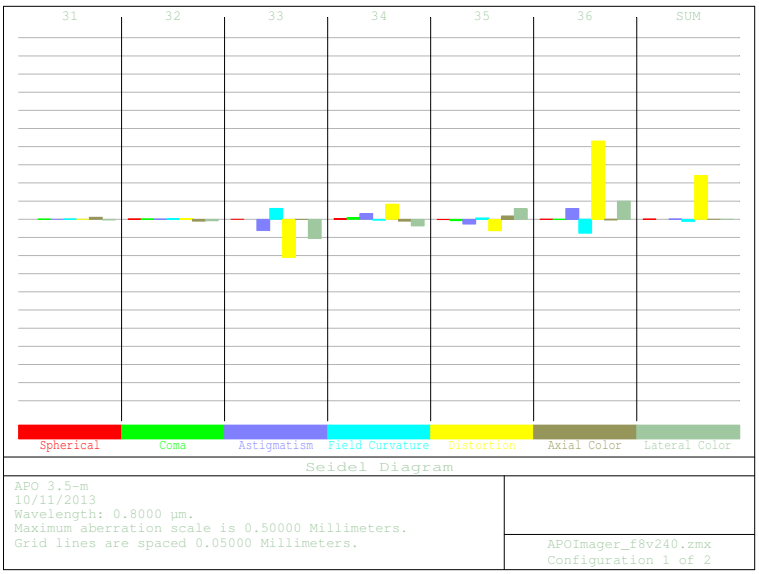

Table 1:: Aberrations

Aberration	Error (waves)
Astigmatism	2.745
Coma	0.060
Spherical	0.155
Distortion	-2.321
Petzval Curvature	0.0002

Ghost focus analysis and re-optimization was performed. Only a sequential mode analysis was performed but future plans include non-sequential modeling of the ghost intensities. Optimization to push the ghost focus and pupil as far away from any surface was performed. The closest ghost pupil, formed from the interaction of surface 36 and 37, is located 11.075mm away from the surface. The closest ghost focus, formed off surface 34 and 35, is located 13.735mm away from the surfaces. All other ghosting is located further away from the respective offending surfaces. The closest distances are far enough from any surface that it will not produce any statically significant photons on the CCD.

An initial tolerance analysis was performed. Further analysis will need to be done to refine the manufacturing tolerances. For the purpose of this document the tolerance analysis shows that standard Zemax tolerances are adequate to ensure good optical performance.

An Inverse Sensitivity Tolerance analysis was performed to check the believability of the initial tolerance conditions. The worst tolerance limits where found in the tilt of L2 and L3. Tilt was expected to be the worse. In these cases the change results in a very small change in the spot radius from the criterion. After verifying the tolerance limits a Sensitivity Tolerance analysis was performed.

The Sensitivity Analysis was run with 41 variables and a Monte Carlo simulation of 10000 trials was chosen to adequately sample the tolerance space. Figure 10 shows the worst results from the simulations. The results are not great, but will have a minimal impact on total system performance. Quality control and compensators will be necessary to mitigate any problems in manufacturing. Mechanical trueness will be checked using a Coordinate Measuring Machine and, along with the manufacturing results, the total offsets should be know and compensated for mechanically.

Fig. 10.—: Tolerance Analysis Worst Spot Diagram

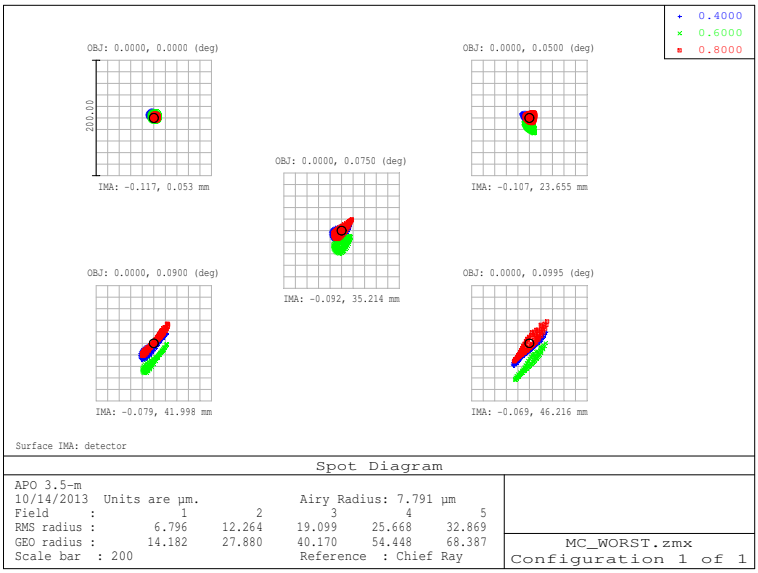

Analysis of thermal changes on the optical stack, with spacers, was performed. Over a temperature range from -20C to 30C (-5F to 85F) the optics stack will shrink by 0.0017 inches and expand by 0.0005 inches. Modeling this in Zemax shows minimal change to spot size, see figure 11. The change in size of the optical stack is the most important since it will change the distance from L3 to the CCD. The CCD will not have any automated piston along the optical axis. Given the small change in performance, no pistoning mechanism will need to be added.

(a) Spot Diagram +30C

(b) Spot Diagram -20C

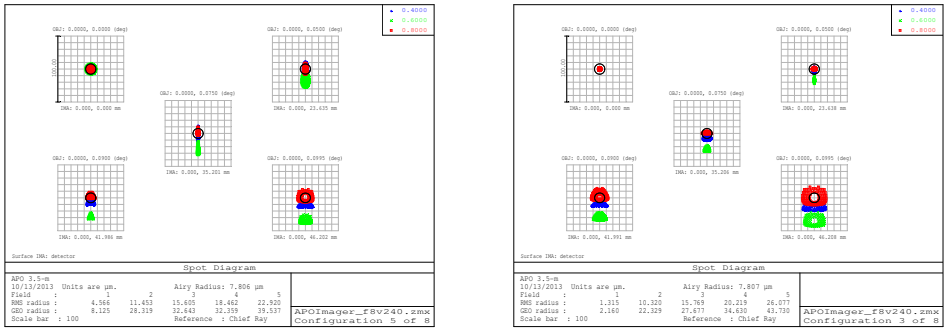

Fig. 11.—: Spot size with respect to temperature

3. CCD

As with any imager, the core of this instrument will be the detector. The e2v chip that would be ideal for the new APO imager is the CCD231-84 back side illuminated detector. This CCD has low read noise (as low as 2 electrons and no higher than 5 electrons). This is, of course, dependent on readout speed. As expected from a science grade CCD, we would also have low dark current (3 electrons/pixel/hour at -100 Celsius).

The clock speed can be set to readout at the fast, higher noise rate or the slow, lower noise rate. The e2v CCD231 has a four channel readout system, see figure 13. At the fastest clock time, 1MHz, the readout can be completed in just under five seconds. Slow readout will take much longer but may be necessary due to science requirements. The readout time described is for 1x1 binning and will decrease by the binning factor. If even faster readout is required a subregion can be selected for readout in a second or two. The readout rate will be selectable between two options set in the software. These will be user selectable through the TUI interface.

Figure 12 shows the electronics noise contribution for a CCD system and electronics identical to what is proposed in the paper. On average the readout electronics add about an electron of noise to the expected CCD noise.

In the optics section the ideal spot size for an f/8 beam was determined to be 40.7μm, yet the e2v CCD231 has 15μm pixels. The detector market has shifted to producing much smaller pixel sizes than when SPICam was first built. A 24μm pixel, such as in SPICam, would be ideal. The only reason a 60mm or greater sized chip with 24μm pixels is not being discussed is that they are not available. The largest off the shelf CCD with a pixel greater than 20μm is 25mm on a side (not necessarily square). As such, the CCD231 will have to be binned to compensate for the oversampling.

The quantum efficiency of this CCD would be high over the entire range if a deep depletion device with the broadband coating is selected, see figure 14 . A peak of 85% in the blue would be seen with the lowest quantum efficiency being about 50% on either end of the spectrum. With an alternate coating a sacrifice in blue quantum efficiency could greatly increase efficiency throughout the remaining range, potentially producing a peak efficiency over 90%.

Deep depletion devices are known to have problems with fringing due to internal reflection of the thinned Silicon. The standard CCD231 has very poor fringing characteristics at wavelengths longer than 750nm. Figure 15 shows that the fringing could be as much as 20% the background level. For an extra 10% the CCD cost fringe suppression can be added. This would decrease the fringe level to a maximum of 2%. Further fringe suppression could be gained by choosing the multi-1 AR coating. This coating will decrease the fringing down to 1% the background level. The current options selected are the astro broadband coating, with fringe suppression. The blue will

[1]Figure 12 plots provided by Bob Leach, Astronomical Research Cameras, Inc.

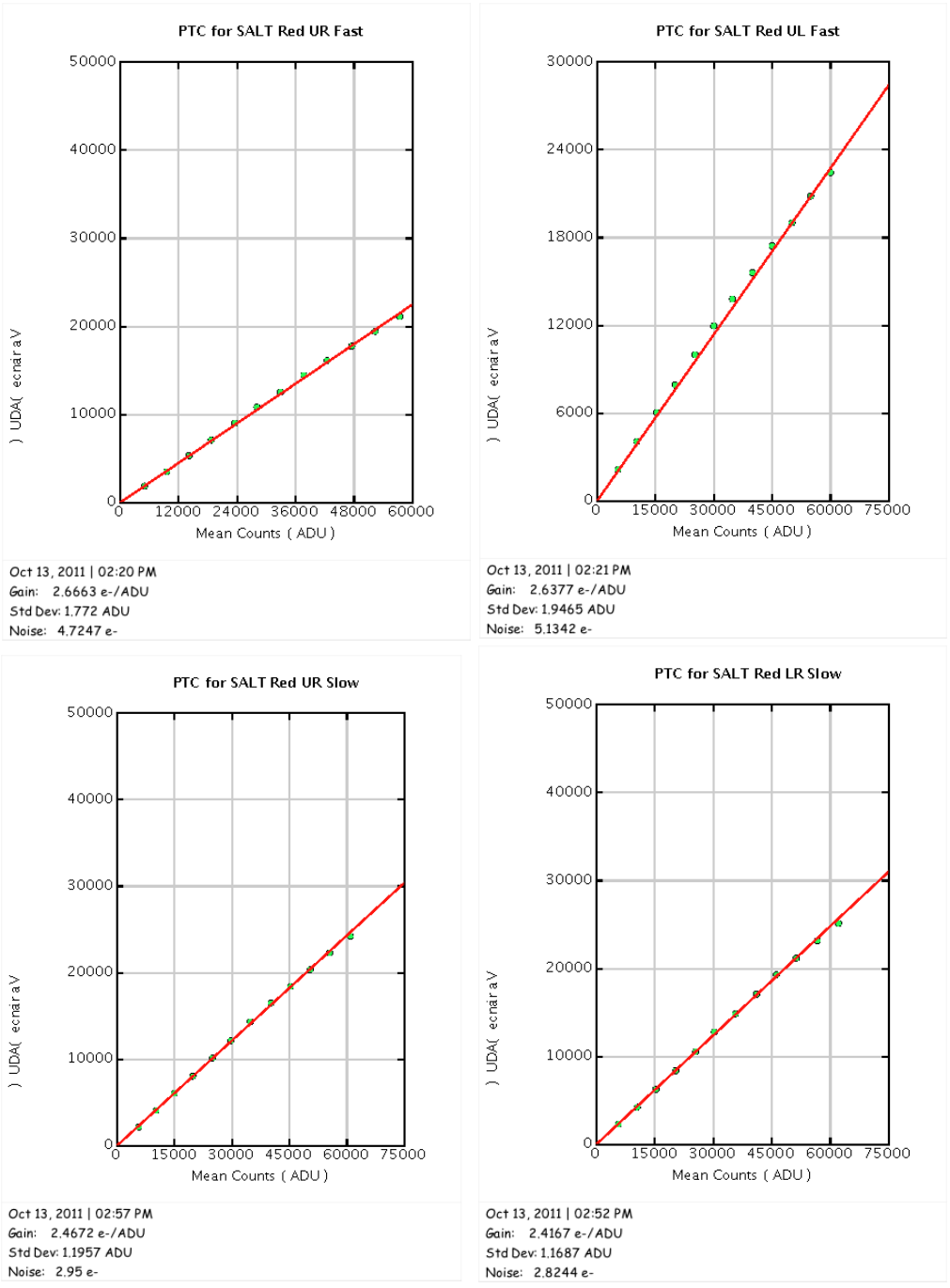

Fig. 12.—: CCD231 Complete Electronics Noise Contributions (top: fast readout; bottom: slow readout)

have better response with good fringe suppression in the red. The costs presented in the PDR reflect these options.

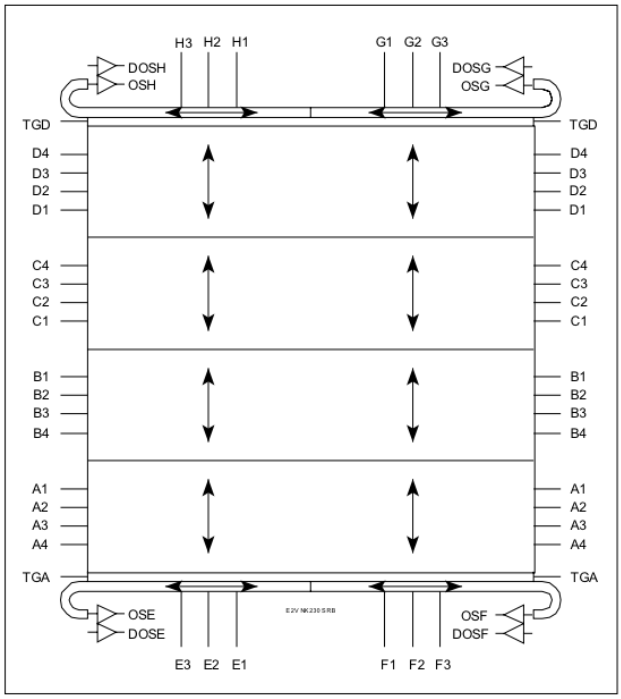

Fig. 13.—: CCD231 Architecture

Fig. 14.—: Quantum Efficiency of CCD231-84

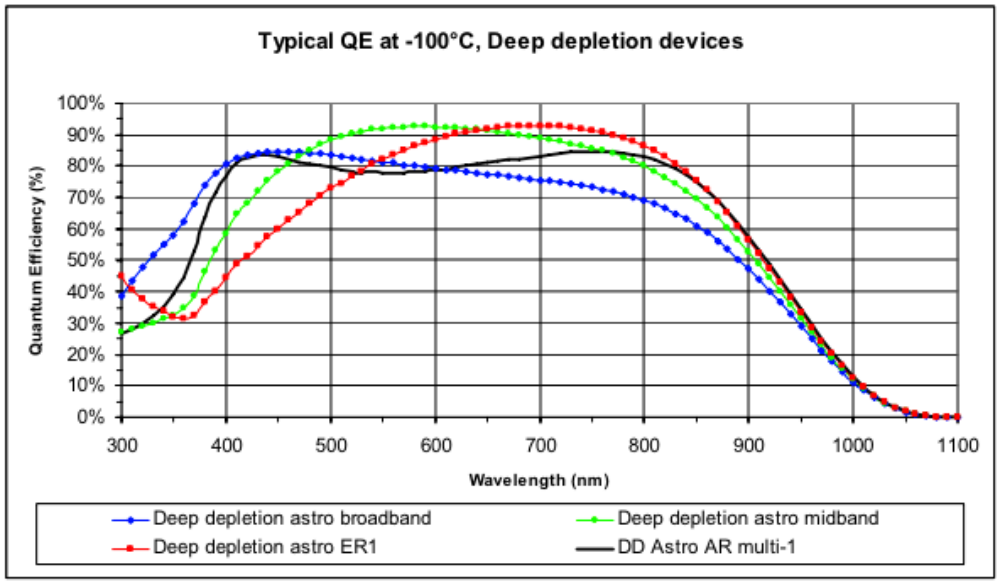

Etaloning in deep depletion astro broadband device

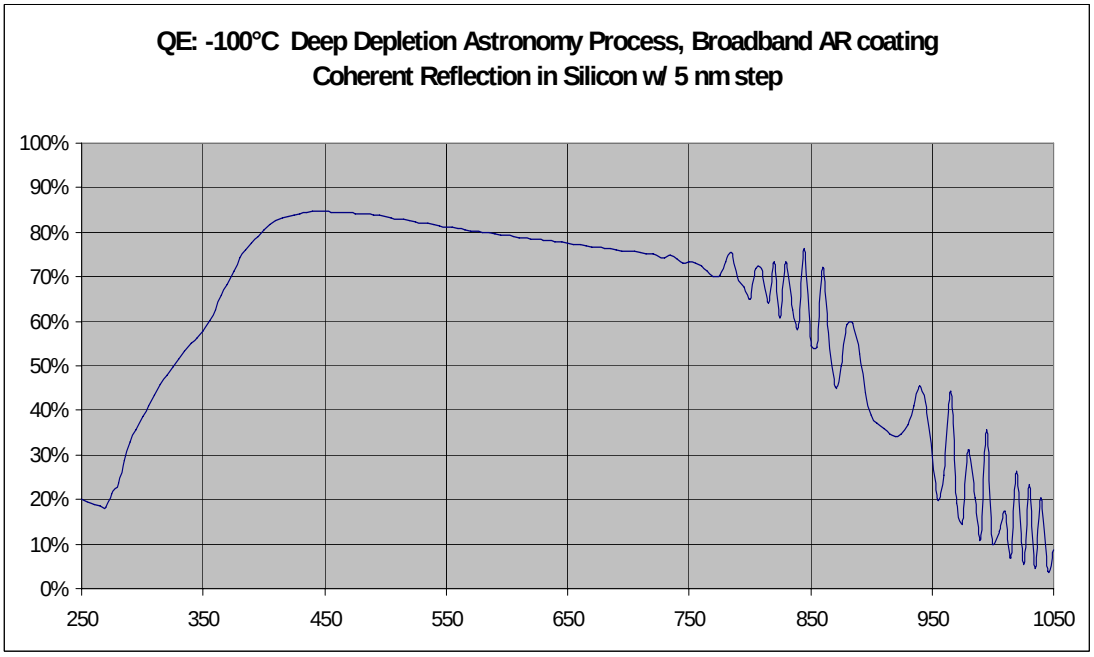

Slide 1

Fig. 15.—: CCD231-84 Fringe Measurement

Table 2:: CCD Comparison

Spec	SPICam	CCD231
Pixel Size	24μm	15μm
Imaging Area	49.1mm^2	61.4mm^2
Read Noise	5.7e$^-$	2e$^-$ - 5e$^-$
Gain	3.36e$^-$/ADU	2.6e$^-$/ADU
Dark Current	2.5e$^-$/pixel/hour	3e$^-$/pixel/hour
Readout Rate	35kHz	1MHz - 50kHz
Readout Time	120 seconds	4.2 - 84 seconds

Notes. Readout Rate and Time only based on 1x1 binning.

4. Mechanical Structure & Filter Wheel

The instrument mechanical structural basis will be essentially two pieces. Initially it was three but an intermediate spacer plate was integrated into the front mounding plate to increase the structural strength as well as decrease the machining time and tolerance stack.

Due to the compactness of the instrument, thermal expansion along the optical axis is negligible. Changes in the CCD position due to temperature changes can be calculated. First, set the initial temperature and boundary conditions. The parts are machined at 18.3C (65F) and a maximum operating temperature from -20C to +30C. There are 6.939 inches of aluminum and 1.050 inches of G10 along the optical axis. Using these numbers it is seen that the CCD will shrink to a minimum size of 7.983 inches and a maximum of 7.991; with a difference over the range of 0.008 inches. Although this is substantial it is easily compensated for by repositioning the secondary mirror to change the distance of the incoming f/10 beam to be further away or closer to the rotator mounting port.

FEA simulations where performed using NX Nastran Structural analysis. The setup started by constraining the assembly through the bolt holes that will hold the components that clamp the instrument to the rotator. Each piece was then mated together through idealized connection assuming perfect joining on the surfaces. A force was then placed along a directional vector. In this simulation +Y is along the optical axis, -Z is towards the top of the instrument, and +X is towards the left of the instrument. Directionality is based on the looking at the instrument as if it was clamped to the telescope instrument rotator. Four analyses were performed with gravitational vectors along major coordinate axes, and two further simulations as if the dewar was pressed on from the sides with a 100 pound force.

The gravitational simulations show good behavior and structural integrity. The purpose of these studies was to see how much flexure would result from gravity. With a goal of less than one pixel of flexure. On the CCD mounting surface it is seen that the flexure ranges from 0.6μm - 1μm. This is well within the 15μm pixel size. The instrument housing was designed to minimize flexure. Each housing piece is thick aluminum with the dewar mounting to the housing through a large flange. The very back of the dewar was allowed to flex since it carries no impact on the CCD position.

For a sanity check, a simulation of what happened if a 100 pound force was placed on the back of the dewar. This causes significantly more flexure but is still acceptable. At the CCD it would flex between 10μm - 16μm. This is not a force I would ever expect the dewar to experience.

Several piece of equipment are attached to the back housing plate. Given the thickness of this plate it is not expected to change flexure. With the instrument filled with equipment it is expected to stiffen up some of the locations of flexure by tying together the structure.

A cart will be built to move the instrument around the observing floor. This will be a welded steel cart made out of box tubing. The instrument will be picked up from the rear of the mounting

Fig. 16.—: Mechanical Structure

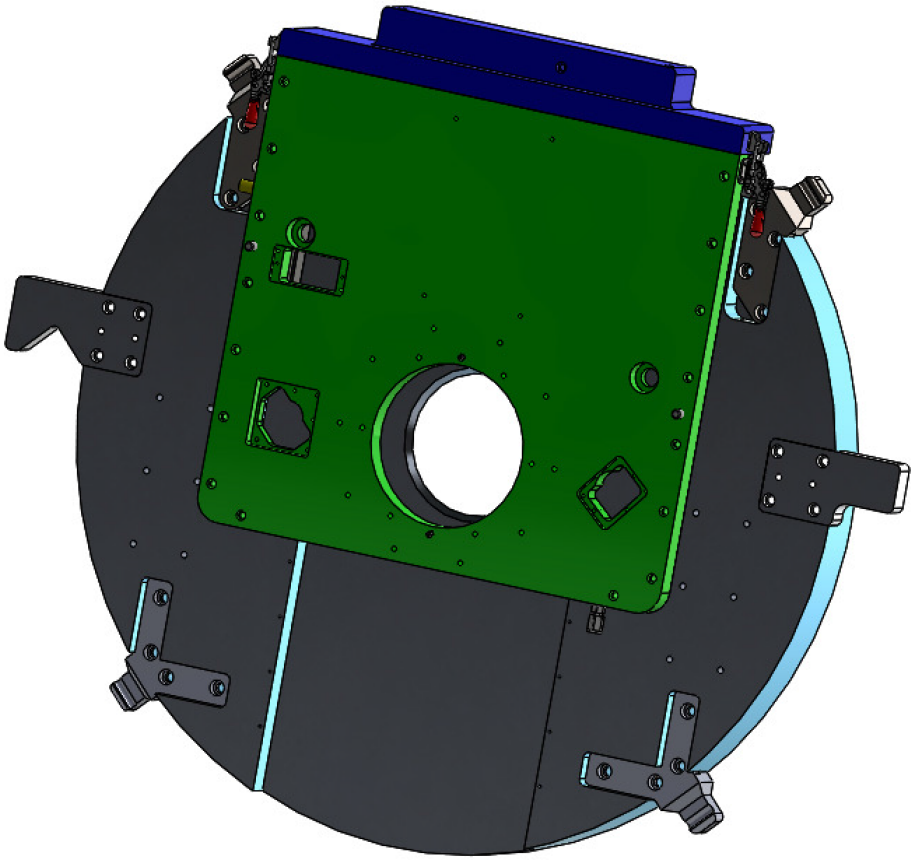

plate (same side as dewar) through a set of linear rods and bearings. It will then slide up and down on the cart through a secondary set of rods and bearings. A linear electric actuator will allow a total range of 12 inches of travel. More information on the cart design will be presented during the PDR.

Fig. 17.—: Simulation Gravitational Vector Up

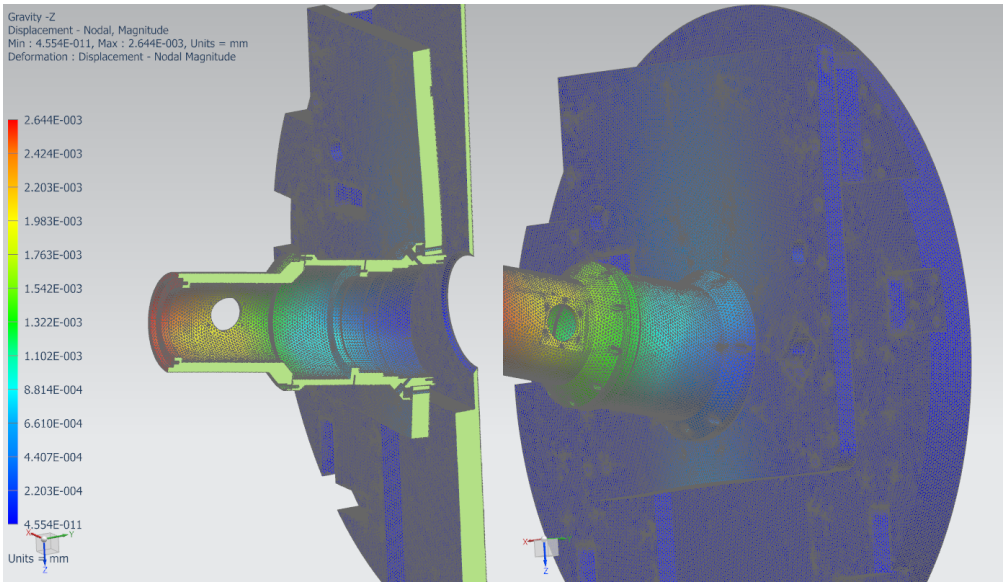

Fig. 18.—: Simulation Gravitational Vector Down

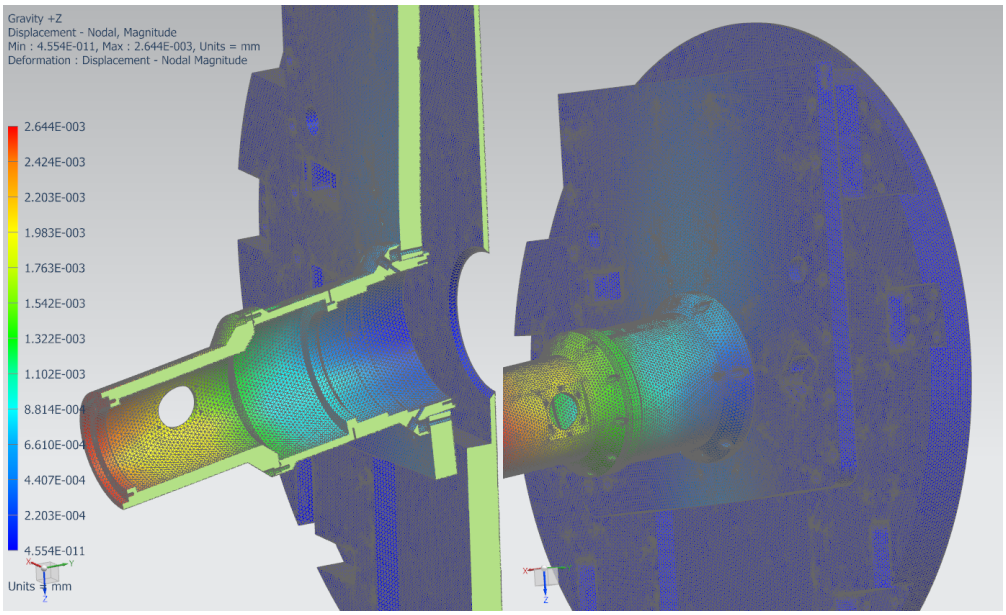

Fig. 19.—: Simulation Gravitational Vector Right

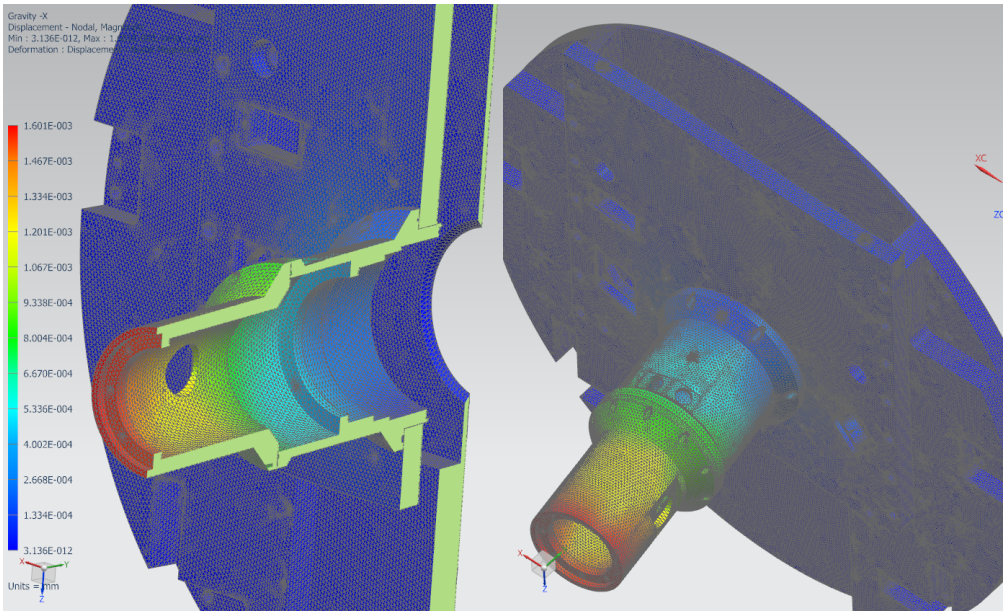

Fig. 20.—: Simulation Gravitational Vector Left

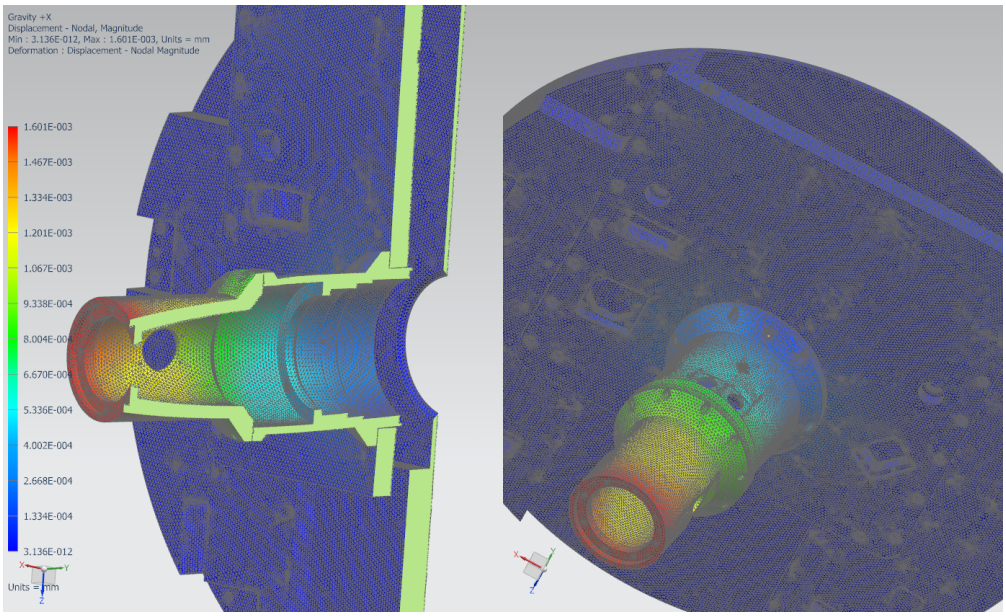

Fig. 21.—: Simulation 100lb Force Down

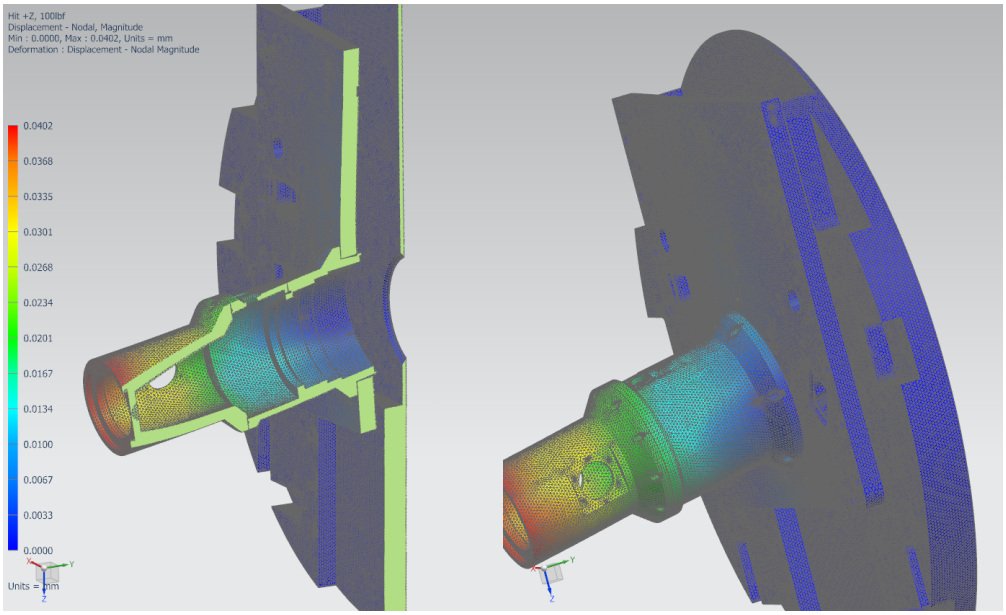

Fig. 22.—: Simulation 100lb Force Right

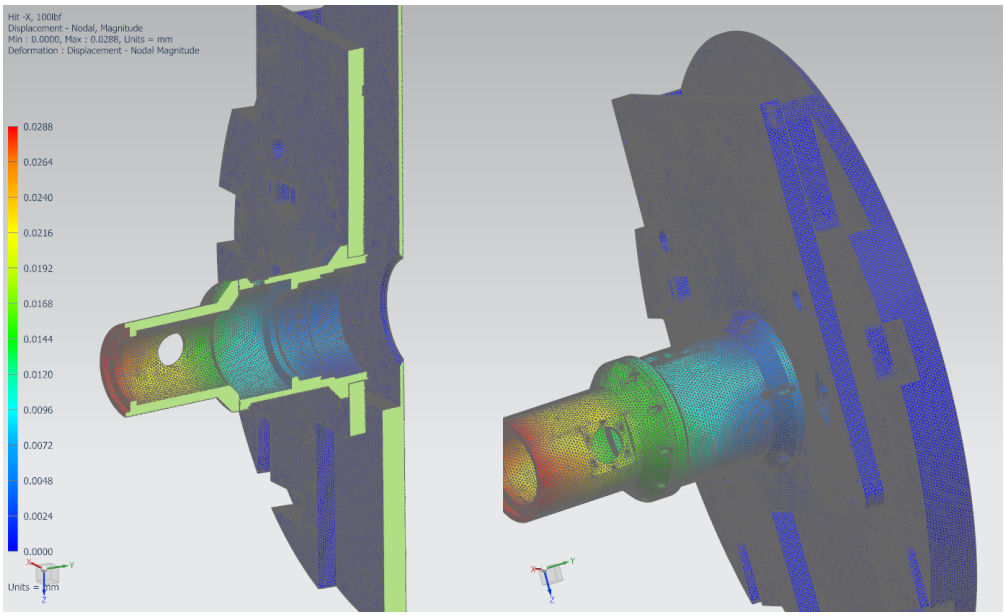

The filter wheel fits into the mechanical structure of the instrument. It is guided into the slots by Delrin runners with 0.01" clearance in each direction. When the filter wheel reaches the end of travel it is captured by the v-groove rollers in the drive mechanics, see figure 23. There is one fixed drive roller, one fixed idle roller, and one tensioning roller. The roller system will contain the filter wheel to within 0.001 inches along the optical axis and with the detents to within 0.04 degrees. Two electric solenoids drive linear detents that will push on dimples in the back of the filter wheel. This will force the filter wheel forward into the drive rollers as well as provide a constant filter position in the rotational direction. The detent dimples can be seen in figure 25. The two detents will be positioned 180 degrees apart to provide an equal pushing force. While driving the filter wheel the detents will be electrically retracted and then when the filters arrives at the position the detents will extend with a spring force. The motor will cut power and the detent will push the filter wheel into a repeatable position.

Positioning and filter wheel identification will be encoded with hall effect sensors. The filter ID is determined by a 4 bit address, this gives room for more filter wheels in the future. The ID bits will be the home position. A bit is then encoded at each position. The stepper will count steps but at the same time look for a positional bit. Ideally, the steps would always be the same, but if slippage occurs the hall status bit will allow for true positional knowledge.

The filter wheel itself will contain a varying number of holes so that an assortment of filters can be mounted. To take advantage of the full field, 5.25 inch diameter filters will need to be used. A total of five large filters will be available at a time. Several filter wheel options will be available. These filter wheels will have adapters to use 3 inch and 2 inch filters along with the larger filters. A total of six filter wheels will be machined by the commissioning of the instrument. These will have varying arrangements of filter sizes based on science drivers. The status bits and detent, described in the previous paragraph, will need to change their physical location on the filter wheel depending on the type of filter wheel. The scheme for controlling filter wheel will be unaffected. The ID bit will let the software know that the filter wheel is of a particular type and how many steps it should move between filters. It will then use the positional status bit to verify the step information.

Fig. 23.—: Filter Wheel Drive

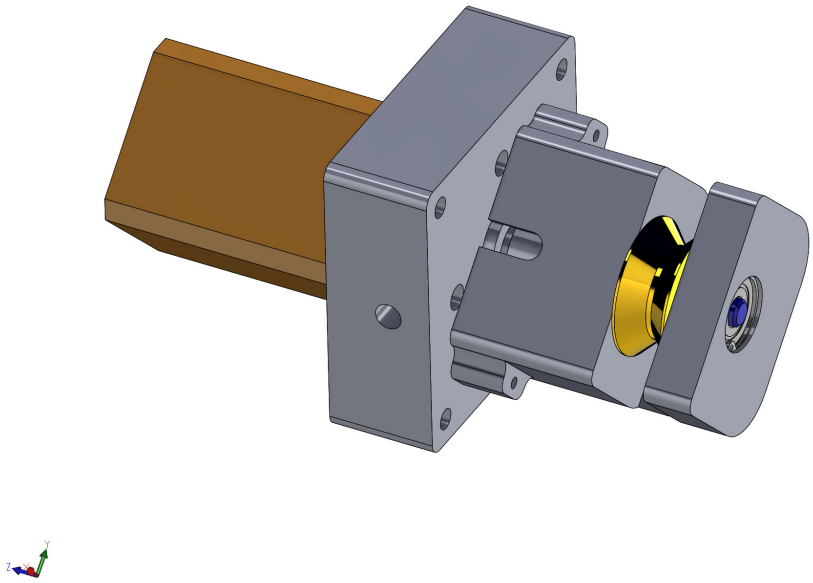

Fig. 24.—: Filter Wheel Assembly

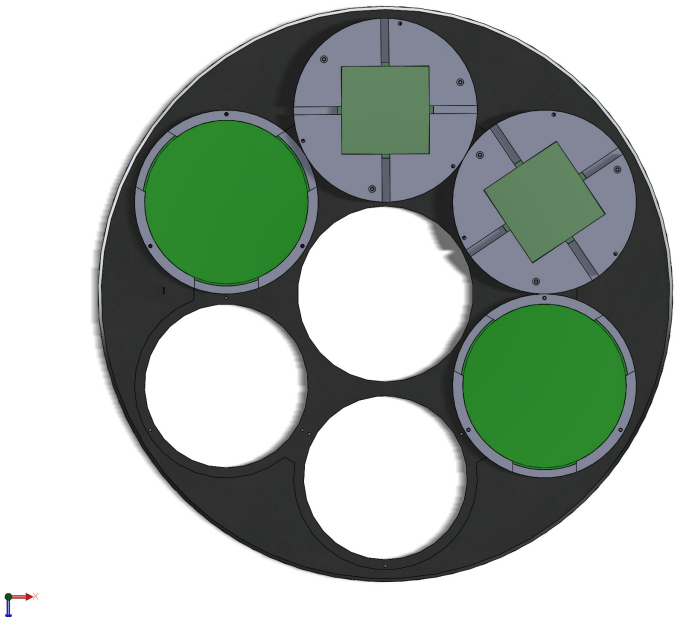

Fig. 25.—: Filter Wheel Detent

5. Shutter

There are many types of shutters available on the market that could be used on this instrument. Instead of buying a shutter, a custom shutter will be designed. This shutter will have several advantages over off-the-shelf options. The basis of these will be: cost, maintainability, and photometric accuracy.

In the long run, the designed custom shutter will cost less than an off-the-shelf option. An iris style shutter that can handle a 5.25 inch diameter aperture will cost on the order of $3K - $5K. These shutters are non-repairable and have a limited lifetime, typically around 100,000 cycles. It is very difficult to find a readily available off-the-shelf version in the necessary size and an iris shutter will create differential lighting across the field. Unfortunately, I don't have numbers for a 140mm diameter shutter, but can use a 90mm shutter for comparison. The stated window time (opening and closing) is 0.112 seconds. This means for an expected minimum continuous exposure of 1 second the differential field exposure will be about 11%. For a maximum expected exposure of 1800 seconds this will be significantly less at 0.006%. But as said earlier this is with a smaller shutter, numbers are expected to be worse for an even larger iris shutter.

To meet the design requirements of high photometric accuracy (I would like to see better than 1% within an 8 arc-minute field) it is necessary to design a custom shutter. The initial manufacturing cost of this shutter will be around $6K, although this is higher than an iris shutter, the components of the custom shutter that are expected to fail will be replaceable. This will decrease the long term costs significantly.

The design of this shutter is a unique, compared to most standard shutters. It will be an independently controlled dual plate shutter driven by an pneumatic cylinder on each plate. The plates will be held in position by a rod and linear bearing system. Each plate will then sit in a recess on its upper and lower edges to control light leakage. The blades will be made of thin carbon fiber with aluminum end caps to add rigidity as well as act as the linkage to the pneumatic cylinder. These blades will be driven by replaceable pneumatic cylinders. Although using a compressible medium as a for an accurate system may prove questionable, it offers several advantages. The first of which is that it will not add heat to the optical path due to the fact that the control solenoids are located outside the instrument. Temperature and pressure telemetry of the air will be monitored and can be used to calibrate the system to known offsets. Hall effects will then monitor the actual exposure time and record the true number in the image fits headers for calibration during image reduction. With all those caveats it should be stated the baseline performance of this type of system.

During lab tests the repeatability of the pneumatic cylinder was around 2ms. There was some stiction seen on the return stroke but it was repeatable to the same 2ms accuracy. Compared to the iris shutter window of 112ms, this is a significant improvement. Significant advantages of this system will be seen with short, repeated exposures. Given that it is a dual plate system with independent control it is possible to create extremely short exposure times independent of the

stroke velocity. With a set stroke velocity of 0.50 seconds the timing of the plates can be such that exposure times less than 1/10 second are possible (with appropriate calibration). This can be accomplished by commanding the closing plate to close 1/10 of a second after commanding the opening plate to open. This differential plate operation and repeatability is what gives this shutter high photometric accuracy across all exposure length ranges.

Solenoid control will be performed by an SMC SY5140 air valve. One of these four way valves will be connected to each pneumatic cylinder. Each valves will output 0.5 Watts of heat but by using a single acting valve only one valve will be powered at each time. The arrangement will be that power will be applied to extend the cylinder. Arranging the cylinders to be in opposing directions means that when one cylinder is extending (using power) the other one will be retracting (not using power). This total of 0.5 Watts will be vented to the intermediate level. Response time of this solenoid is 32ms. But since this is a constant it will only play a role in the continuous frequency of operation. A minimum recommended frequency will be around 2Hz, although work is still being done to squeeze out more performance.

The maintainability of this system will also be significantly easier and more cost effective when compared to other shutter types. The entire shutter unit will be removable from the instrument. If cylinders need to be replaced it should take, on the order, about 30 minutes. The current cylinder that is being tested is a Bimba double acting cylinder. These cylinders should probably be replaced every other year. More robust cylinders, such as Air-Pel, are also being researched but are significantly more expensive and the lifetime is not known.

The shutter mechanism is fit into the instrument via a hole in the bottom of the instrument housing. It is then guided into position by two locator pins and tensioned on the opposing end via a torque limiting screw. The shutter is as close to the first lens of the dewar as possible, to minimize light leaks, but it is not coupled to the dewar, to minimize vibration transfer. It is not believed that vibration from the shutter will transfer through the housing into the dewar, but several provisions are taken. The pneumatic cylinders will have internal bumpers as well as springs external to the cylinder to decelerate the plunger at the end of travel. This will prolong the life of the cylinder while providing smooth operation.

Fig. 26.—: Shutter View 1

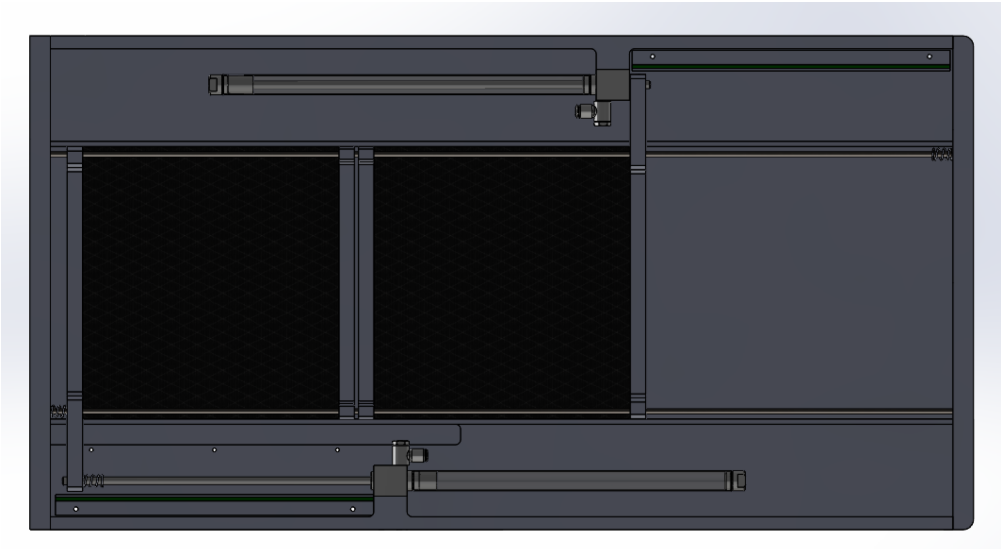

Fig. 27.—: Shutter View 2

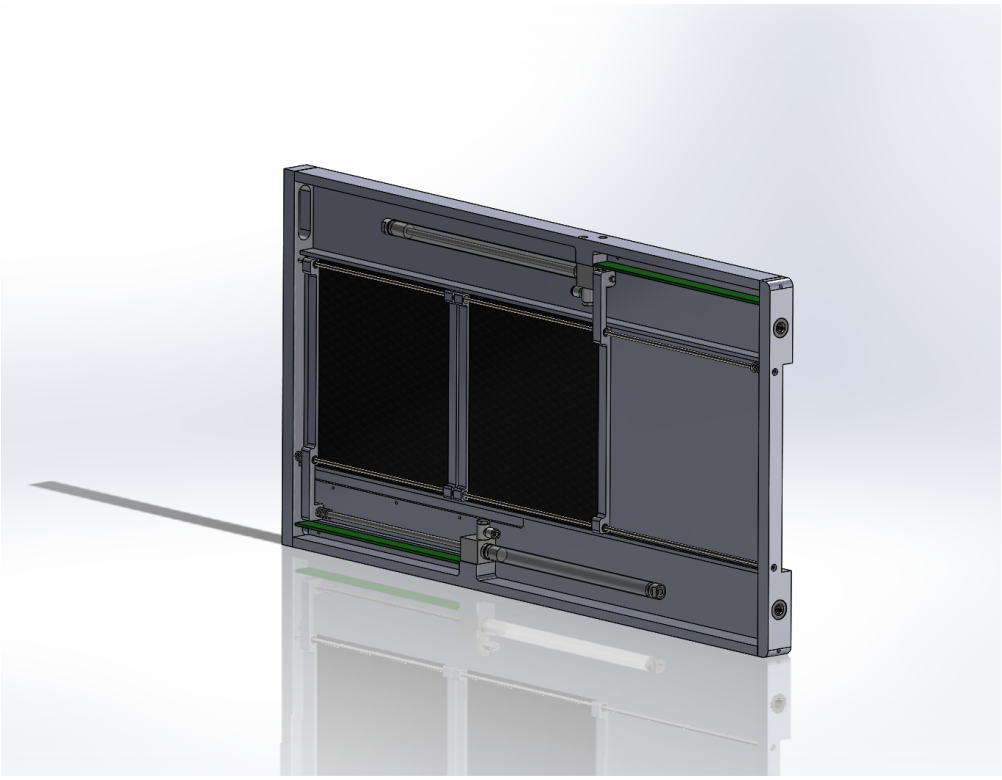

6. Dewar

6.1. Body

Choice of the dewar was one that was researched early on in this project. Off the shelf options, such as IR Labs, were considered but the cost vs included benefits was too high. A custom dewar was designed to create a compact and feature-full dewar. The dewar consists of two body components. The back half houses the PCC cold head while the front half contains the CCD subsystem and optical elements. A single housing could not be made due to the diametrical difference between the cold head and the CCD subsystem. The mating point between the two was placed such that it would be easier to machine all the components.

The rear section of the dewar will have a smaller internal diameter compared to the front section to decrease the total internal surface area of the dewar. It will also contain three vacuum ports. On the rear will be the seating port for the PCC cold head which will extend past the opposite end of the dewar into the front dewar section vacuum cavity. The cold head is machined with the o-ring groove in the cold head section so no o-ring groove will be necessary on the back section. The two remaining vacuum ports will be equivalent to KF40 in size, located on opposing sides, towards the front of this section. One port will be attached to a vacuum valve and serve as the pump access point. The other port will contain the telemetry. To minimize adapters (and o-rings) a custom brazed tee made of SS304L will be connected to this vacuum port. On one side of the tee will be an MKS 972 series vacuum gauge. This gauge is a cold cathode/micro-pirani style that can read from atmosphere to $1x10^{-8}$ Torr. Vacuum readings are available through an RS-232 interface. The opposing side of the tee will hold the ion pump. A current version to what is on SPICam will be used. This will be a Gamma Vacuum TiTan, 3 litre/sec, ion pump. The differential version is capable of pumping on noble gases with a reduction in inefficiency by 20%. Given the small size of the dewar this will not be a problem and could prove more beneficial in the long term.

The front section of the dewar will be the most complex. It will contain the focal reducing optical elements, CCD substructure, and electrical feedthroughs. The vacuum portion of this dewar will contain three blind tapped holes for mounting of the CCD substructure. The rear mounting flange will contain an o-ring groove for a 5.99 inch ID, 0.103 inch cross section Viton oring. The window o-ring will be the same but with a 4.74 inch ID. The front and rear sections of the dewar will be mated using 10 - #10 screws evenly spaced around the o-ring groove. On the atmosphere side of the dewar will be the focal reducer stack. This stack will contain the three optical elements in stepped cavities. To minimize the amount of glass necessary each element has a small outer diameter in the progression of the converging beam. The element closest to the CCD will act as the dewar window. This previously mentioned o-ring will seal against a flat polished lip on the last surface. Each element will have a glass reinforced polycarbonate spacer along the optical axis. This will evenly space the elements with a plastic that has a close matching coefficient of thermal expansion. On the exterior of the dewar will be an inlet and outlet hole between each optical element to flow

Fig. 28.—: Dewar

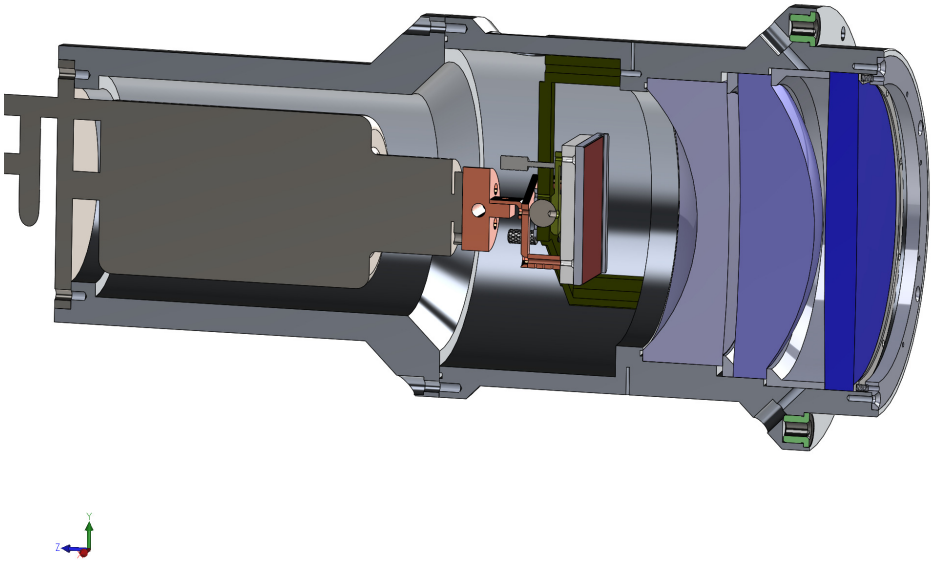

dry air through the space. The forward most air fitting is located on the chamfer of the matting flange. The diametrical constraint of each lens will be held my machining tolerances. Given the optical tolerances this is more than adequate. The stacked elements will be constrained on the front surface by a set of compression springs held evenly around the diameter. These springs will press against a mating polycarbonate piece so as not to touch the glass. The distributed spring force will be around 20lbs which will account for the weight of the optics stack while providing movement for minor shock events and appropriate movement in hopefully unforeseen circumstances.

The dewar will mount to the instrument body by 6 - 1/4 inch bolts. Holding the dewar into position will be two hardened locator pins and bushings placed on opposing sides of the mating face. Locator bushings will be on the dewar sections so that the dewar can be rested on its front face for maintenance. Diamond locator pins will be placed in the instrument housing. Each pin will locate one axis, given the shape, and with an arrangement of two pins the dewar will be tightly constrained but should not be over constrained so as to make it difficult to assemble.

The o-rings were chosen to be Viton due to a compromise between the outgassing and permeation characteristics. Table 3 shows some defining statistics. Weight loss is an indicator of outgassing. Buna N shows significantly more outgassing while only a slightly improvement in permeation over Viton. There will be a total of eight vacuum seals on this instrument. One of which

Fig. 29.—: Dewar Optical Stack

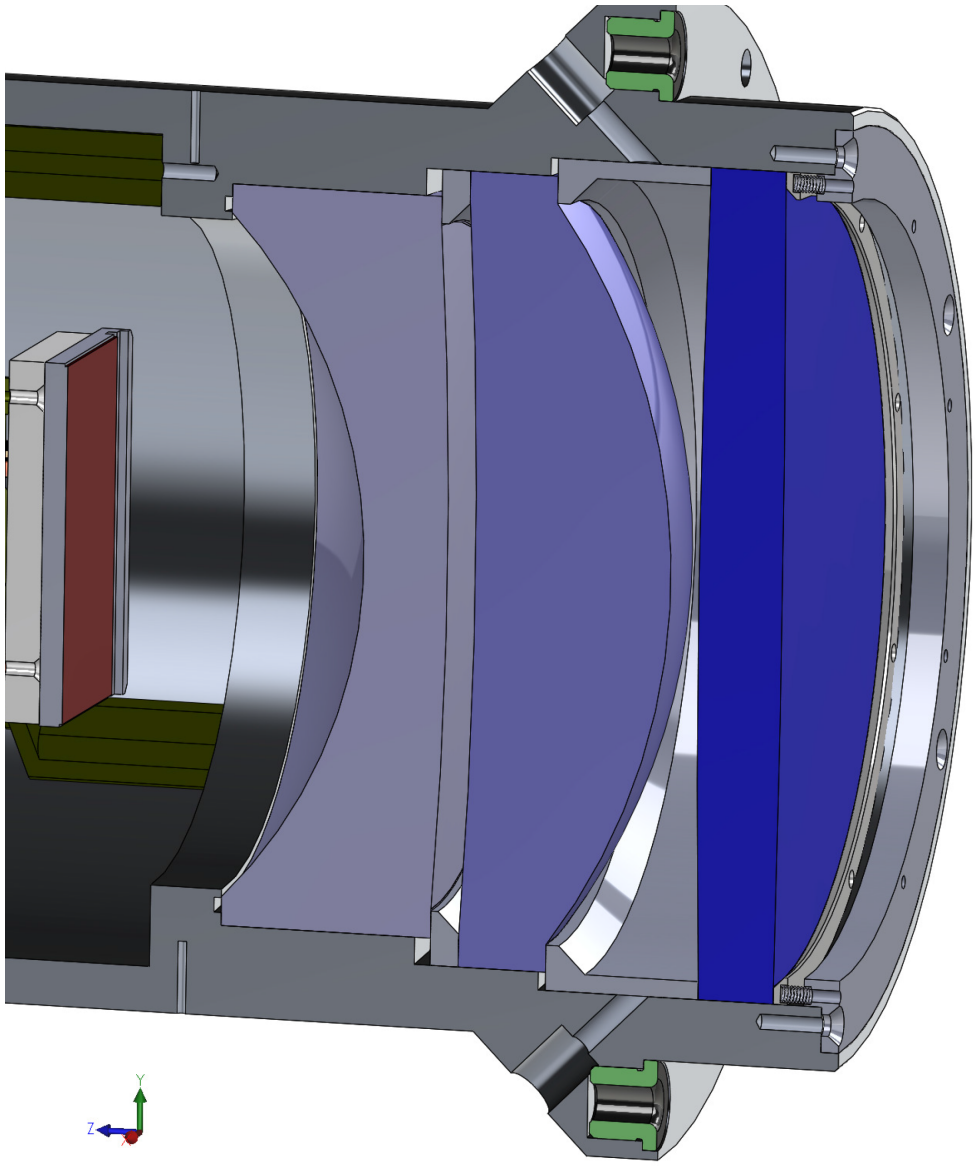

is a small ConFlat seal.

[2]Information obtained from Meyer Tool and Manufacturing, Inc.

Table 3:: O-Ring Statistics[2]

Material	Name	Weight Loss (%)	He Permeation	N_2 Permeation
Flourocarbon	Viton	0.07	$8x10^{-8}$	$0.18x10^{-8}$ - $1.9x10^{-8}$
Nitrile	Buna N	1.06	$12.7x10^{-8}$	$0.23x10^{-8}$

6.2. CCD Substructure

The CCD is held in place through a G10 spider with tip/tilt adjustment. The main G10 spider is the contact point between the warm dewar wall and the cold CCD. It also is the carrier for the tip/tilt mechanism. The tip/tilt is performed through a concentrically placed ball bearing that is captured through the top of the G10 spider. A single bolt in the ball bearing is used as the mating point of the receiving spider that attaches to the Aluminum Nitride cold plate. Tip and tilt is accomplished by three 4-48 thumb screws. Spacings are such that the range of motion is around 5 degrees. The thumb screws will provide tension to tilt the CCD but locking it in place is performed by the backing plate on the captured ball bearing. By tightening this backing plate the ball bearing will be over constrained and prevented from moving.

Aluminum Nitride was chosen as the cold plate for several reasons. These being: material matching of CCD package, good thermal conductivity, and good electrical isolation. The AlNi block will be attached to the CCD structure through the G10 ball attachment. It will also be independently coupled to the cold, copper spider. This spider will move independently from the tip/tilt mechanism and is the connecting point from the cold plate to the cold strap.

The cold strap will be minimal in size to produce a colder cold tip than CCD. The cold tip will be mated to the cold strap via a copper block that will house the heater. A rough temperature control heater will be placed away from the cold head so that the thermal variation across the CCD is not affected. There will also be a temperature sensor on this cold tip adapter.

Three temperature sensors will be used in the dewar. One will be placed in near the cold tip, and two on the cold plate. Of the two sensors on the cold plate one will be redundant. The temperature sensors chosen will be silicon diodes from the Lakeshore Cryogenics DT-670 product line. A strain relief will be built around the sensor casing to protect the sensor wires as they exit the sensor. Thermal anchoring of the sensor wires will then be performed on the cold plate and cold tip adapter, which ever is closest to the sensor.

6.3. Thermal Analysis

Thermal analysis was performed using NX 8.5 Thermal Simulation with a steady state solution. A load of 1.2 watts was placed on the CCD while a thermal anchor of 173 Kelvin was placed on the upper section of the cold tip attachment. The legs of the G10 spider at the mating point of the

dewar were anchored to 273K. Figures 31 - 33 show temperature variations throughout the spider structure, cold strap, and across the CCD.

Figure 31 shows that nearly no heat is transferred to the outside world. Although the G10 structure does cool as the closer to the contact point of the cold plate it does not transfer much thermal energy from the outside world.

Figure 32 shows that there is a temperature differential of about four Kelvin between the CCD and the cold tip. This was done by minimizing the cold strap to make sure the CCD is always warmer that the cold tip so that any water in the dewar will condense on the cold tip well before the CCD. A heater will be placed on the cold tip attachment to ensure a consistent operating temperature of the CCD between 165K and 175K.

The main heat load in the dewar will be the CCD. Figure 30 shows the heat produced by the combined amplifiers during readout. This, of course, is dependent on readout speed. Our maximum readout frequency will be 1MHz. At the maximum heat load the temperature differential across the CCD is about 0.06K, figure 33. This of course is an idealized situation with steady state temperatures.

Fig. 30.—: CCD Amplifier Thermal Load

Readout frequency	Line time	Amplifier load	Power dissipation			
			Amplifiers	Serial clocks	Parallel clocks	Total
100 kHz	21 ms	10 kΩ	165 mW	17 mW	3 mW	185 mW
1 MHz	2.2 ms	5 kΩ	275 mW	170 mW	30 mW	475 mW
3 MHz	800 µs	2.2 kΩ	525 mW	510 mW	90 mW	1,125 mW

Cooling of the dewar will be accomplished using a Brooks Automation Polycold Compact Cryocooler (aka Cryotiger). This system has a possible range of temperatures dependent on the thermal load, see figure 34. The CCD is intended to run around 173K, but more importantly, it should be very temperature stable. Given diurnal temperature swings and cooling efficiency changes it will be necessary to PID control the heater on the cold tip attachment to maintain a constant temperature. The cold tip heater will affect large temperature changes and a small heater on the cold plate will account for any minor temperature changes. Temperature control will be tuned to regulate the temperature to within ±0.5K. Temperature feedback will be through two silicon diode temperature sensors (with one wired backup). These sensors will feed the Lakeshore temperature controller to achieve the desired temperature.

It is still undecided what will happen to the interior wall of the dewar. Currently there are two options: Nickel plating and thermal blanketing. A polished and plated dewar wall with a 0.0005 inch layer of Nickel would decrease radiation to the outside world. The expected emissivity of a Nickel plated wall would be 4%. Another option would be to use a thermal shielding material, such

the material used in TripleSpec. This material is a mylar sheet that is coated on each side with an aluminum layer. This will provide a physical thermal insulation of from the interior of the dewar to the outside world as well as create a constant emissivity (exact numbers are not known). With the low cost of plating and large thermal overhead, Nickel plating is planned.

Table 4:: Estimated Thermal Load

Item	Heat Load (Watts)
CCD	1.125
2 x Temperature Sensor	(2x) 1.0 x 10^{-5}
Wires	0.5
Substructure	0.5

Fig. 31.—: Temperature differential through Warm Structure

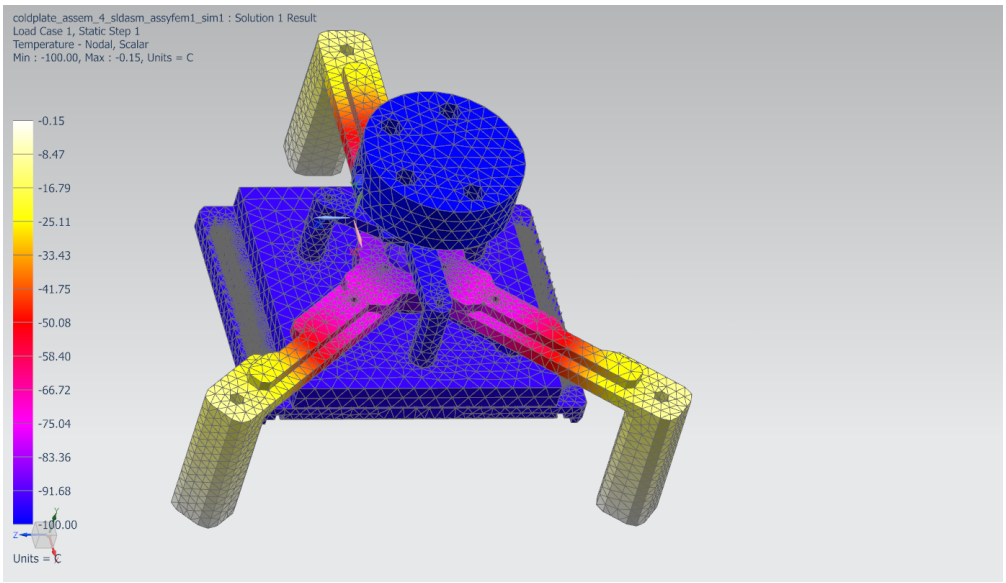

Fig. 32.—: Temperature Differential on through Cold Strap

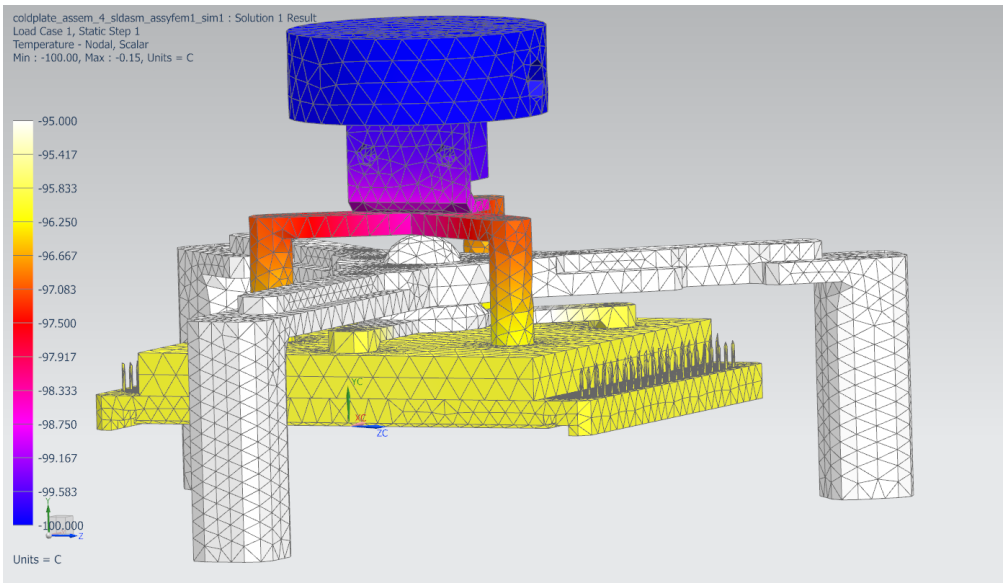

Fig. 33.—: Temperature Differential Across CCD

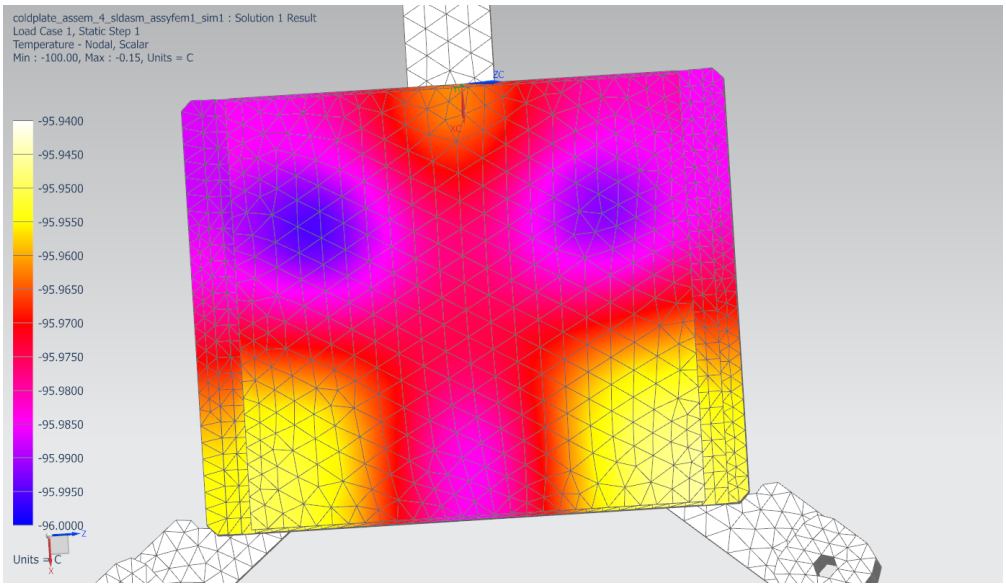

Fig. 34.—: PCC Cooling Capability, PT-30